Seismic transmission tomography: determination of the elastic properties of building structures (some examples)

Ettore Cardarelli
Dipartimento Idraulica Trasporti e Strade, Università di Roma «La Sapienza», Roma, Italy

Abstract
This paper is a general review on seismic transmission tomography considering data acquisition and processing. Some questions on linear and non linear inversions are tackled, and advice given on the choice of the best damping factor. Taking into account prediction matrices we show that it is possible to point out the best distribution of sensors and shot points in terms of resolution and stability of system. Then two examples in which seismic tomography was used are described concerning the determination of elastic characteristics of building structures.

Key words *applied geophysics – cultural heritage – inversion – seismic tomography*

1. Introduction

The prefix *tomo* is Greek for *slice* and therefore implies a 2D reconstruction of the field of an elastic characteristic (velocity and/or attenuation) of a material (natural ground or structures) using elastic waves that cross it.

Seismic tomography, depending on the type of used wave, can be divided in reflection, diffraction, transmission and refraction tomography. It is known that seismic tomography shows different aspects and problems depending on the types of survey carried out. For this reason, seismic tomography can be divided into deep and shallow tomography, depending on the depth of investigation.

This paper deals with transmission tomography because this is usually used in shallow surveys that are mainly targets of engineering applied geophysics.

Shallow high resolution tomography is generally employed as a tool for determining the elastic properties of rock masses involved in large civil engineering projects and as a particular application for detecting and characterising mechanical discontinuities in the main structures of ancient monuments and important buildings. These surveys generally investigate zones having dimensions ranging from one meter up to a few tens of meters and velocities that may change from 300 m/s to 3000÷4000 m/s.

In these surveys measurement errors play an important role with respect to deeper surveys because the absolute value error is always independent of travel-time value. Furthermore, we have to consider that dealing with smaller travel-time values, a high percentage errors occurs, which are the errors related to the ill positions of shots and geophones, and the reading errors of the picking of the first breaks. The reading errors are due to the attenuation of the signal because of the high frequency loss that can depend, in the case of building structures, on bad coupling between the investigated structure and the sensors and the noise that may be elec-

Mailing address: Prof. Ettore Cardarelli, Dipartimento Idraulica Trasporti e Strade, Università di Roma «La Sapienza», Via Eudossiana 18, 00184 Roma, Italy; e-mail: ettore.cardarelli@uniroma1.it

tric random noise due to recording device and electric coupling in seismic cables, or external noise caused by wind, rain and factors that depend on human activities.

2. Background

Suppose we have a set of observed travel times, $t_1, ..., t_m$, from m sources-receivers pairs in a medium of slowness $s(x) = 1/v(x)$ where $v(x)$ is the wave velocity. Let P_i be the Fermat ray path connecting the ith source-receiver pair. Neglecting the errors, we can write

$$\int_{P_i} s(x)\, dl^{P_i} = t_i \qquad i = 1, \ldots\ldots m. \qquad (2.1)$$

Given a model of slowness, let l_{ij} be the length of the ith ray path through the jth cell and given a model with n cells (fig. 1) above equation can be discretized and written as:

$$\sum_{j=1}^{n} l_{ij} s_j = t_j \qquad i = 1, \ldots\ldots m. \qquad (2.2)$$

If now we write the previous equation in matrix notation by defining the column vectors $\boldsymbol{s}$ and $\boldsymbol{t}$ and the matrix $\boldsymbol{M}$ as follows:

$$\boldsymbol{s} = \begin{pmatrix} s_1 \\ s_2 \\ . \\ . \\ s_n \end{pmatrix} \quad \boldsymbol{t} = \begin{pmatrix} t_1 \\ t_2 \\ . \\ . \\ t_n \end{pmatrix} \quad \boldsymbol{M} = \begin{pmatrix} l_{11} & l_{12} & \ldots & l_{1n} \\ l_{21} & l_{22} & \ldots & l_{2n} \\ . & . & \ldots & . \\ . & . & \ldots & . \\ l_{m1} & l_{m2} & \ldots & l_{mn} \end{pmatrix}$$

The previous equation becomes the basic equation of forward modelling for ray analysis

$$\boldsymbol{Ms} = \boldsymbol{t}. \qquad (2.3)$$

The formal solution follows:

$$\boldsymbol{s} = \boldsymbol{M}^{-1}\boldsymbol{t}. \qquad (2.4)$$

Since generally $\boldsymbol{M}$ is not square *we have to find some type of solution.*

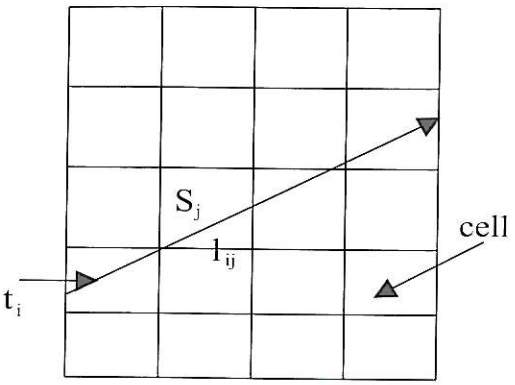

Fig. 1. Seismic transmission tomography. t_i is the travel time that the ray-path spends travelling from shot point to sensor. s_j is slowness of jth cell. l_{ij} is the length of the ith ray-path in the jth cell.

At this moment we have to define the meaning of the forward and inverse problem.

The forward problem determines the predicted data ($\boldsymbol{t}^{\text{pre}}$) when model parameters ($\boldsymbol{s}^{\text{true}}$) are defined using $\boldsymbol{M}$ whilst the inverse problem evaluates model parameters ($\boldsymbol{s}^{\text{est}}$) starting from a data set that constitutes the

$$\boldsymbol{t}^{\text{pre}} = \boldsymbol{M}\boldsymbol{s}^{\text{true}} \qquad (2.5)$$

observational data ($\boldsymbol{t}^{\text{obs}}$) by using the inverse $\boldsymbol{M}^{-1}$

$$\boldsymbol{s}^{\text{est}} = \boldsymbol{M}^{-1}\boldsymbol{t}^{\text{obs}}. \qquad (2.6)$$

3. Inversion

All inversions can be divided on a relationship between a small perturbation to the model and its effects on observations (data) and from the relationship that links the unknowns with the data set. Under this hypothesis the inversion may be linear or non linear.

In our case, we are dealing with a linear problem so that the (2.4) or a derivation from (2.4) is used.

In the case in which the problem is not linear but can be linearized around a reference model it is not possible to solve the problem by (2.4) or its derivation but the non linear operator must be linearized by using a first order expansion Taylor series in which if $G(x)$ is the non linear operator and x_0 is the reference model we can write $G(x) = G(x_0) + B_0(x - x_0)$ where $\boldsymbol{B}$ is the derivative operator with

$$\boldsymbol{B}_0 = \left| \frac{\partial G}{\partial x} \right|_{x_0} .$$

Linear Inversion

Considering a non negative functional defined as

$$\Psi(\boldsymbol{s}) = (\boldsymbol{t} - \boldsymbol{M}\boldsymbol{s})^T(\boldsymbol{t} - \boldsymbol{M}\boldsymbol{s}) \qquad (3.1)$$

it can be regarded as the sum of the squares of the residuals. If $\Psi \equiv 0$ we solved our problem, if $\Psi \neq 0$ then we did not solve our problem, but for small Ψ we are close to solving it. Taking the derivative of Ψ with respect to $\boldsymbol{s}$, we find $\boldsymbol{s}$ that gives the minimum value of the squared error

$$\boldsymbol{M}^T\boldsymbol{M}\boldsymbol{s} = \boldsymbol{M}^T\boldsymbol{t}. \qquad (3.2)$$

This is known as the normal equation for least-squares, and the matrix $\boldsymbol{M}^T\boldsymbol{M}$ the normal matrix. If we are dealing with an overdetermined problem and this is generally the case, *i.e.* $m > n$, and we may assume that the inverse exists, also if this usually is not true, a formal solution can be given from

$$\boldsymbol{s} = [\boldsymbol{M}^T\boldsymbol{M}]^{-1}\boldsymbol{M}^T\boldsymbol{t} = \boldsymbol{M}^{-g}\boldsymbol{t} \qquad (3.3)$$

Where $\boldsymbol{M}^{-g}$ is the generalised inverse of our inversion.

If $[\boldsymbol{M}^T\boldsymbol{M}]^{-1}$ is singular the previous equation cannot be solved and a new functional $\Psi^I(s)$ has to be considered

$$\Psi^I(s) = \Psi(s) + \lambda s^T s \qquad (3.4)$$

where the weighting factor λ determines the relative importance given to the prediction error $\Psi(s)$ and solution length $L = s^T s$. If λ is made large enough, this procedure will minimise the undetermined part of the solution. If λ is set to zero, the prediction error will be minimised but no *a priori* condition will be provided to single out the undetermined model parameters.

It is, however, possible to find some value for λ that will minimise $\Psi(s)$ while will minimising the length of the undetermined part of the solution.

4. How can we solve the problem?

There is no simple method of determining what kind of compromise we have to choose to detect λ. If we minimise with respect to the model parameters in the same way as the least squares derivation, we can write

$$\boldsymbol{s} = [\boldsymbol{M}^T\boldsymbol{M} + \lambda\boldsymbol{I}]^{-1}\boldsymbol{M}^T\boldsymbol{t}. \qquad (4.1)$$

This solution is called the damped least squares solution and λ the damping value. It may be determined by a trial and error process which weighs the relative merits of having a solution with small variance against those of having one that fits the data and is well resolved.

In some cases, it is possible to detect the best damping factor analysing the trend of mean square deviation σ_t between the field travel times and the theoretical ones. It can be demonstrated that the best λ will be detected when the first significant increase in the diagram σ_t (the knee of the curve) (Bernabini and Cardarelli, 1987) is obtained (fig. 2).

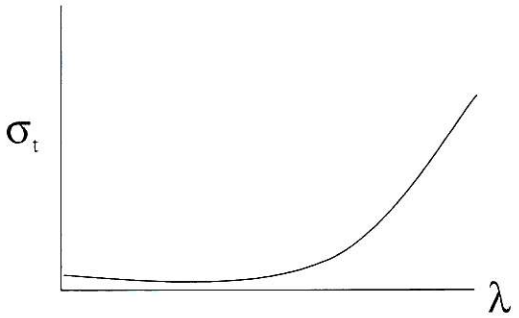

Fig. 2. Trend of σ_t depending on the damping value λ.

Further considerations can be made about the damping factor.

It is possible to demonstrate that the lower velocity cells are more robust and react to the damping factor by introducing perturbations in the velocity field of the investigated area. To avoid this, the damping factor should be relaxed in the low velocity zones and boosted in the high velocity ones. For this reason, instead of considering constant damping factors, variable ones can be introduced and lower coefficients may be assigned to lower velocity cells (Bernabini and Cardarelli, 1997). Under this hypothesis eq. (4.1) was modified as

$$s = [M^T M + \Lambda^T]^{-1} M^T t \qquad (4.2)$$

where the matrix Λ is a diagonal matrix in which damping factors are the diagonal elements.

There are many cases where the solution length $L = s^T s$ is not a good measure of solution simplicity. If the more probable value of the investigated slowness is s^*, the solution length can be written as

$$L = (s - s^*)^T (s - s^*).$$

In this case, taking advantage of *a priori* information (3.4) can be modified as

$$\Psi^{\|}(s) = \Psi(s) + \lambda (s - s^*)^T (s - s^*). \qquad (4.3)$$

If we minimise $\Psi^{\|}(s)$ with respect to the model parameters in the same way as the least squares derivation, we can write

$$s = [M^T M + \lambda I]^{-1} M^T t + [M^T M + \lambda I]^{-1} \lambda s^*. \quad (4.4)$$

This is the equation where the information *a priori* s^* is considered. It may be utilised if mean elastic characteristics of the investigated material are known. If s^* is set to zero, the above equation coincides with (4.1).

If variable dampings are considered (4.4) can be modified as

$$s = [M^T M + \Lambda^T]^{-1} M^T t + [M^T M + \Lambda^T]^{-1} \Lambda^T s^*. \qquad (4.5)$$

This equation gives best results in those cases where low velocity cells exist (high slowness).

4.1. *Algorithms used*

In general, there is no optimum algorithm for any problem, every survey is a new problem where the choice of the best algorithm has to be determined considering the characteristics of inversion with respect to those of the survey.

The algorithms can be divided depending on the operative way to process data: direct, iterative, quasi-iterative and stochastic.

In direct methods we can include, Gauss-Jordan elimination and Singular Value Decomposition (SVD), these algorithms are generally used for linear problems with few equations and few parameters (unknowns).

In the iterative methods we may consider the Algebraic Reconstruction Technique (ART), Simultaneous Iterative Reconstruction Technique (SIRT) and Conjugate Gradient (CG) methods; these algorithms are usually utilised for problems with a large number of equations and unknowns where large sparse matrices occur, because the direct methods take too much computer memory space, these algorithms are generally utilised although they are more time consuming. Iterative methods are also used for non linear problems where a set of linearised steps is necessary to reach the minimum of error criterion function.

In the quasi-iterative methods, the least QR factorisation (LSQR) and Lanczos methods can be considered, these algorithms can be used for both linear and non linear inversions depending on the properties of the algorithms that we are dealing with.

Finally, in the stochastic methods all the Monte Carlo methods may be included, mainly Simulated Annealing. These methods are generally used to solve the highly non linear problems when it is not possible to linearise them.

Because, in general, shallow seismic tomography deals with few parameters and faces linear problems, principally direct methods are utilised such as the Gauss-Jordan elimination and the SVD. The SVD is generally used to perform analysis of the system in order to determine if it is well or ill conditioned by using the ratio between the higher and the lower eigenvalue (condition number) and spectra analysis of eigenvalues and eigenvectors of the generalised

inverse of the system. Equation (4.4) written in the SVD formalism is

$$s = V \operatorname{diag}\left[\frac{w_j}{w_j^2 + \lambda}\right] U^T t + \\ + V \operatorname{diag}\left[\frac{\lambda}{w_j^2 + \lambda}\right] V^T s^* \quad (4.6)$$

where U is the eigenvector matrix that spans data space, V is the eigenvector matrix that spans the space of unknowns and w_j are the eigenvalues of generalised inverse of the system.

In the case in which some singular values are zero, the W matrix of singular values can be rearranged in a diagonal submatrix W_p of p non zero singular values. This operation is equivalent to decreasing the number of unknowns until the p value is reached. In such a way, the system becomes overdetermined and can normally be solved.

In the 3D case and when the system is ill-conditioned, we generally use the LSQR algorithm (Paige and Saunders, 1982) because with respect to the iterative methods it gives a smaller residual for the same number of iterations and is more robust. The explanation for this might be that with CG we deal with normal matrix ($M^T M$) whereas in the LSQR approach we deal only with the matrix M (Van der Sluis and Van der Vost, 1987)

For non linear problems the Biconjugate Gradient is generally used, this being a special version of conjugate gradient. The ordinary CG method works well for matrices that are well conditioned, *i.e.* «close» to the identity matrix. The strategy of these algorithms consists in multiplying matrix M with a *preconditioner* M^* close to M in which case $M^{*-1} M \cong 1$ allowing the algorithm to converge in fewer iterations because it is necessary to avoid 'many' CG iterations in order not to increase noise.

4.2. *Resolution*

In shallow seismic tomography, one important target is the resolution of the field velocity that we need. The resolution depends on two important parameters: the number of unknowns and the dimensions of cells in which the investigated area is divided. The first parameter is directly linked to the number of equations *i.e.* the number of unknowns cannot overcome the number of equations, in the least squares sense, the second parameter is linked to the fundamental frequency of the seismic wave that travels in the investigated area. In fact, the Fresnel ray theory (Cerveny and Soares, 1992) suggests the minimum dimension of the object that we can detect by

$$R_F = \frac{1}{2}\sqrt{\frac{dv}{f}} \quad (4.7)$$

where d is the distance between shot point and sensors v is the mean velocity of the investigated area and f is the fundamental frequency of the recorded seismic wave and R_F is the ray Fresnel. For this reason the minimum dimension of cell that we can consider will be equal to R_F.

Considering that the elastic characteristics of the medium are affected by mean characteristics of the elements of volume having dimensions $\approx \lambda/2$ if $R_f < \lambda/2$, for short distances, the minimum dimension to consider will be $\lambda/2$, where λ is the wavelength.

4.3. *Is it possible to plan a survey?*

There are many possibilities to arrange the position of sources and sensors with respect to the distribution cell but it is necessary to predict which is the best disposition to avoid amplifying measurement errors.

To face such a question prediction matrices can be used. Because these matrices depend only on distribution of shot, sensor points and arrangement of grid cells, in the straight ray-path approximation, they can be analysed and studied before performing the survey.

Model resolution matrix MRM

The MRM defined as ($M^{-g} M$) (Menke, 1989) indicates if a model can be independently pre-

dicted or resolved. In fact if we consider that

$$s^{est} = M^{-g} t^{obs} \qquad t^{obs} = M s^{true}. \tag{4.8}$$

Substituting in the first of (4.8) the second we obtain

$$s^{est} = [M^{-g} M] s^{true}. \tag{4.9}$$

(4.9) suggests that the estimated parameters are equal to the true ones when $(M^{-g}M)$ is equal to the identity matrix.

Data resolution matrix DRM

The DRM defined as (MM^{-g}) (Menke, 1989) indicates if data can be independently predicted or resolved, considering

$$s^{est} = M^{-g} t^{obs} \qquad t^{pre} = M s^{est}. \tag{4.10}$$

Substituting in the second of (4.10) the first we obtain

$$t^{pre} = [MM^{-g}] t^{obs}. \tag{4.11}$$

Also in this case (4.11) suggests that the predicted data are equal to the observed data if DRM is equal to the identity matrix.

Unit covariance matrix UCM

The unit covariance matrix is defined as

$$\mathrm{UCM} = (M^T M)^{-1}. \tag{4.12}$$

This matrix, under the hypothesis of uncorrelated data, by the analysis of its main diagonal provides the degree of error amplification that occurs in the inversion and analysing the elements off the main diagonal gives the correlation degree between each cell with respect to all the others.

4.4. *Acquisition device*

In shallow seismic tomography the high resolution is one of the most important factors determining the quality of the results. In this frame the acquisition device plays an important role because a good choice of recording sample rate, cut-off frequency of sensors and interdistance between the sensors and shot points can determine the success of a survey.

In the survey that we are describing data acquisition was carried out with a sample rate of 100 μs and piezoelectric sensors with a cut-off frequency of 4 kHz. As a source a hammer of about 2 kg was utilised. Because of the short recording times we used the technique that, in addition to the trigger of the seismograph, uses the shot time (Bernabini *et al.*, 1990). The trigger of seismograph is activated by the hammer that interrupts an electrical circuit during its course toward the shot point. The shot time is recorded through a piezoelectric sensor assembled within the hammer, which is then connected to a channel of the seismograph. In this manner, we are able to read travel times as the difference between the shot instant recorded on the channel connected to the piezoelectric sensor of the hammer and the first breaks of each channel (fig. 3).

5. Two case histories

In order to summarise and for a better understanding of the previous sections two examples of high resolution seismic transmission tomography for determination of elastic characteristics of building structures will be shown.

5.1. *Application of 3D and 2D seismic tomography on some samples of building panels (1st example)*

This survey (Cardarelli and de Nardis, 1998) was carried out to verify if seismic tomography can be a valid tool to acquire of knowledge of the elastic properties of brick walls and their variations when walls are subjected to different loads.

The survey was performed on building panels that were expressly erected with the techniques of ancient Roman buildings. We executed the experiment subjecting panels to different loads.

During these tests we carried out seismic tomography to reveal elastic variations that arose

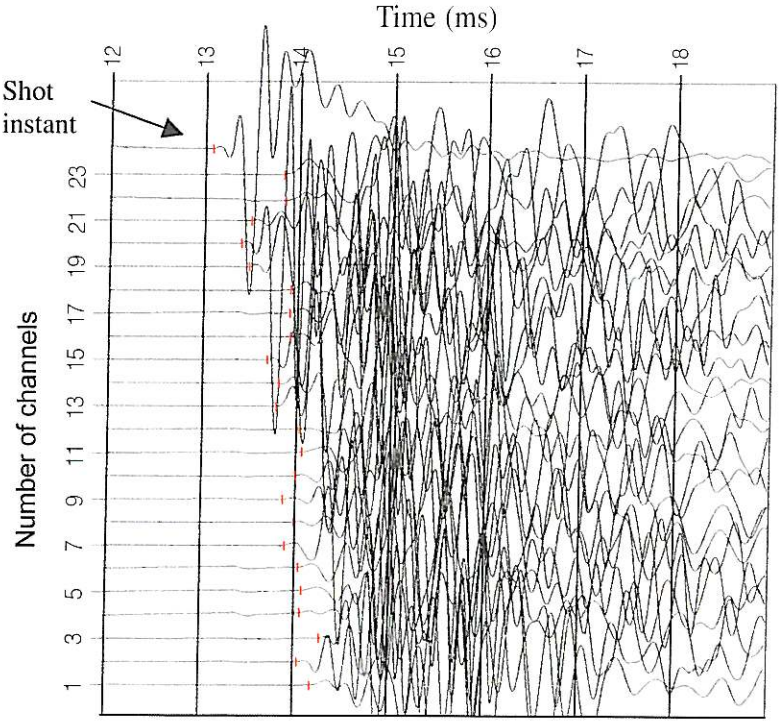

Fig. 3. Seismic tomography record. Shot instant is indicated and the picking is performed.

from different loads and to predict possible cracks or fractures.

The experiment, that surveyed the wall, was divided into four load phases, each one using a different load.

The building panels measured $1 \times 1 \times 0.45$ m^3. The inversion was performed in 3D and 2D projection. We divided the panel into 18 voxels (3D cells) and used 345 ray-paths for 3D survey and 12 pixels (2D cells) and 120 ray-paths in 2D case. The LSQR algorithm for 3D and the SVD for the 2D inversion were used. The 2D inversion was performed only taking into account the ray-paths with the same z co-ordinates *i.e.* considering seismic waves that travelled on the same plane that coincides with the plane where sensors and shot points were located.

Figures 4a-d and 5a-d show the results of 3D and 2D inversion, in these figures it is possible to distinguish elastic differences between different load phases. Observing fig. 4b, in the 2nd phase when the load increases to 45 kg/cm^2 an improvement of elastic characteristics with respect to the 1st phase (fig. 4a) is shown, probably because the load increases the stiffness of the wall. When the load decreases to zero in the 3rd phase (fig. 4c), it is possible to note that the elastic characteristics decrease with respect to the 1st phase because first permanent deformations arose. In the 4th phase (fig. 4d) when the load increases to 60 kg/cm^2 the elastic characteristics of the wall improve but do not reach the mean values that the wall showed in the 1st phase to demonstrate that permanent deformations have arisen. Increasing the load to 62 kg/cm^2 the wall was disrupted and open fractures were visible on the right bottom side of the wall where the lower velocities were detected.

Considering that the fractures were parallel to the load, we performed 2D inversion because the rays travelling perpendicularly to the fractures could enhance the elastic differences dur-

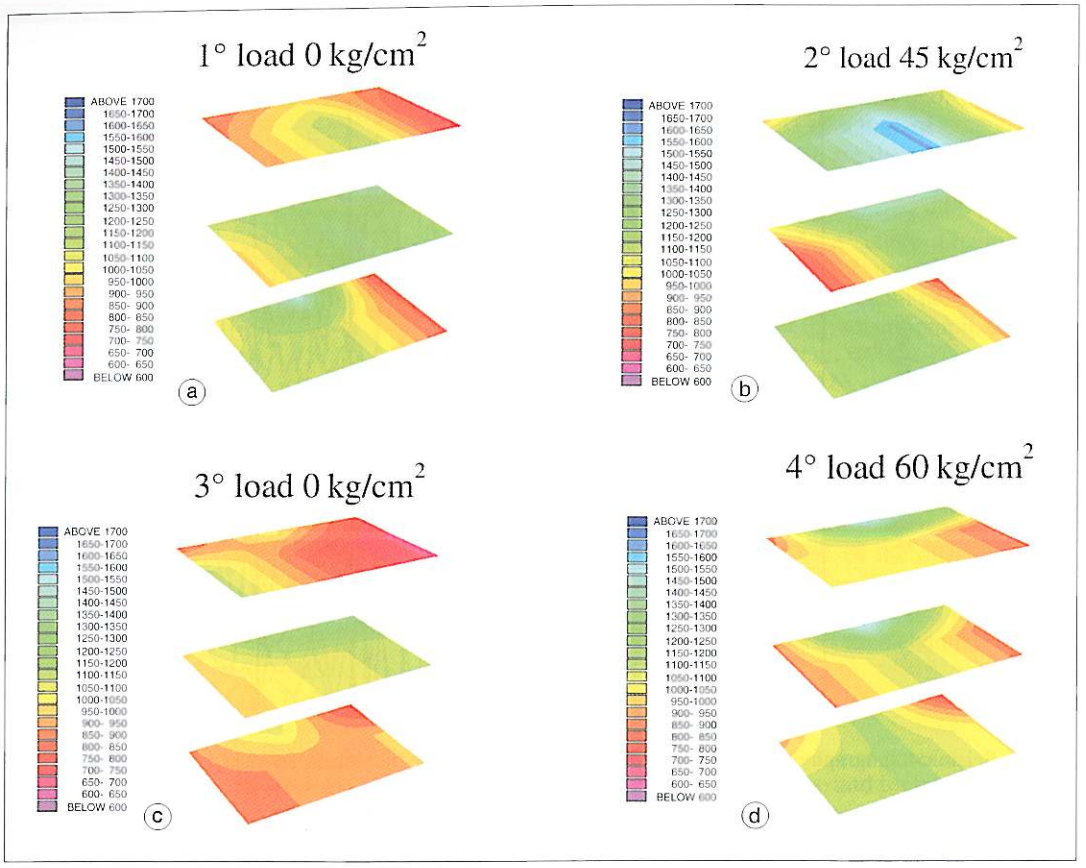

Fig. 4a-d. 3D inversion results (after Cardarelli and de Nardis, 1999).

ing the different phases. In fig. 5c in the 3rd phase the low velocities are better detected with respect to 3D representation.

From the results we can conclude that it is possible to use seismic tomography as a tool to detect different elastic characteristics in brick walls that are subjected to different loads.

5.2. *Seismic refraction, isotropic and anisotropic seismic tomography on an ancient monument (2nd example)*

This survey was performed on three columns of the pronao of Antonino and Faustina Temple (141 A.D.) (Cardarelli and de Nardis, 1998). The columns are formed of cipollino marble that is made up of mica and calcite beds. The columns are 15 m long and have a diameter of about 1.5 m The goal of the survey was to determine the decay degree of the columns of the Temple in order to give information to the restorer to plan the restoration. To test a methodology that takes into account different geophysical techniques to integrate the results, two seismic techniques were performed. At first, the survey was carried out by seismic refraction and seismic tomography on two columns. In fig. 6 the arrays of seismic refraction and seismic tomography are shown. In each column two lines of seismic refraction were performed in opposite sites for each spread of 12 geophones,

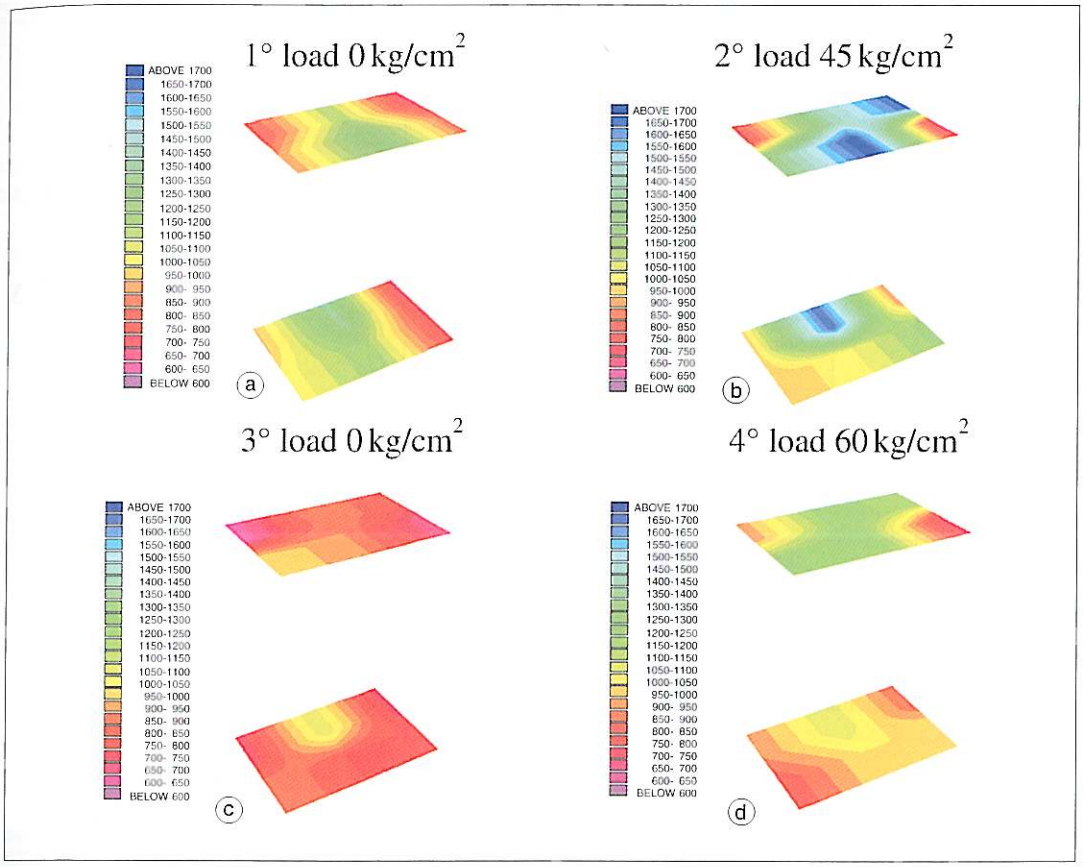

Fig. 5a-d. 2D inversion results (after Cardarelli and de Nardis, 1999).

having an interdistance of 25 cm between one another, 5 shots were located as is shown in fig. 6. Seismic tomography was performed dividing the columns into four parts. In each part, 23 sensors were located distributed as shown in the figure, between the sensors shot points were located. Seismic refraction was processed using the delay times method (Gardner, 1939) and then adapted as suggested by Bernabini (1965). Seismic tomography was processed by the LSQR algorithm (Paige and Saunders, 1982) both 3D and 2D inversion. Since the 3D tomography did not give significant results a 2D inversion was performed. Figures 7 and 8 show the results of seismic refraction and 2D tomography. Both surveys indicate that the columns, considering velocity values, may be divided into three zones: in the tomographic survey a weathered zone, where the velocities range from 0.4-0.6 km/s, an intermediate zone characterised by velocities ranging from 0.8-1.2 km/s, an inner zone where the velocities reach the values 2-2.5 km/s. In the refraction survey the weathered zone is characterised by velocities that are more or less the same as those detected by tomography, in the intermediate zone the velocities range from 1.5-2.5 km/s and finally the inner zone shows the highest velocities from 3.5 to 5 km/s. The different elastic behaviour detected between the two techniques was interpreted as anisotropic behaviour of the cipollino marble. The reason for this is that in

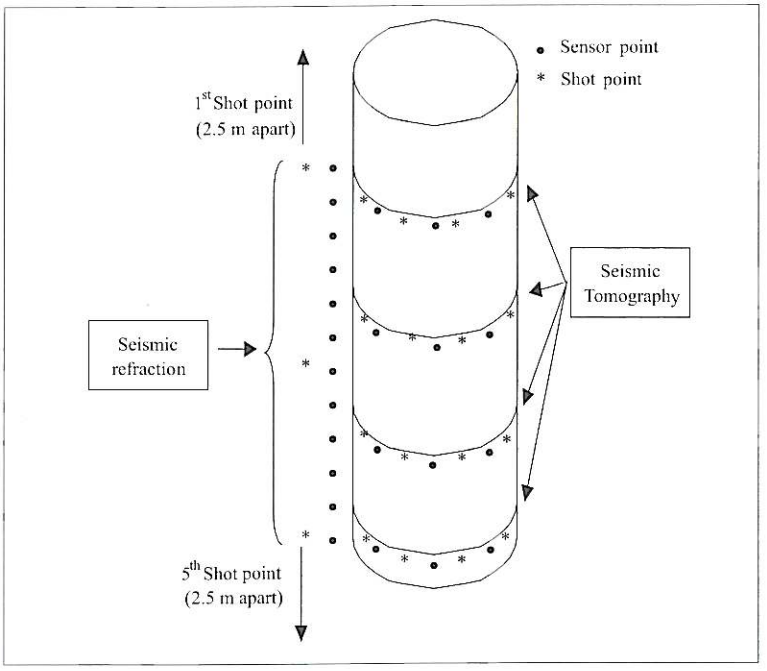

Fig. 6. Seismic refraction and seismic tomography array (after Cardarelli and de Nardis, 2001).

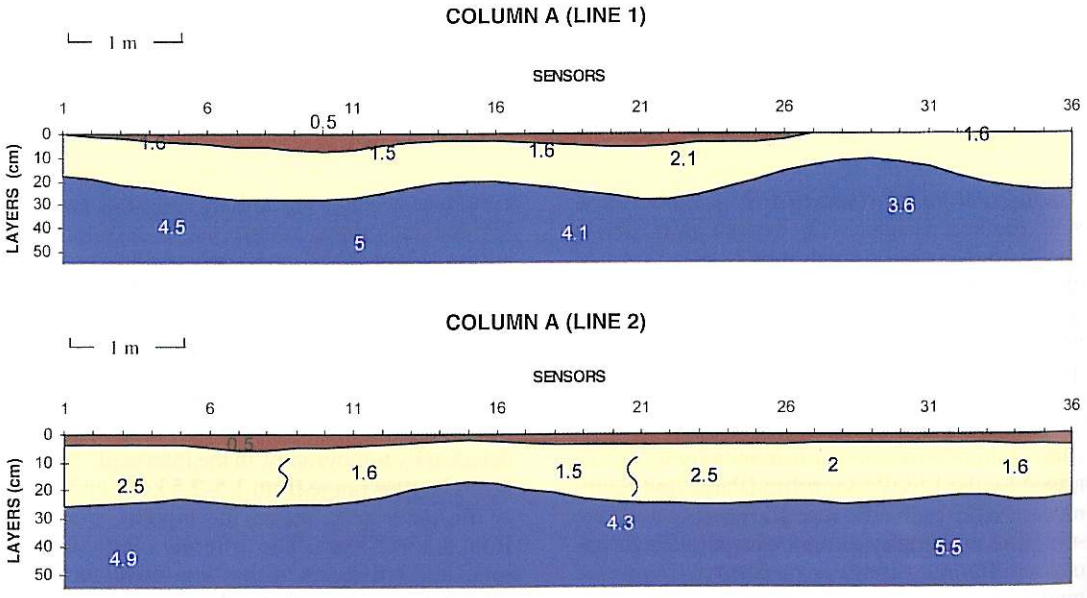

Fig. 7. Seismic refraction results of Column A. Velocities are in km/s (after Cardarelli and de Nardis, 2001).

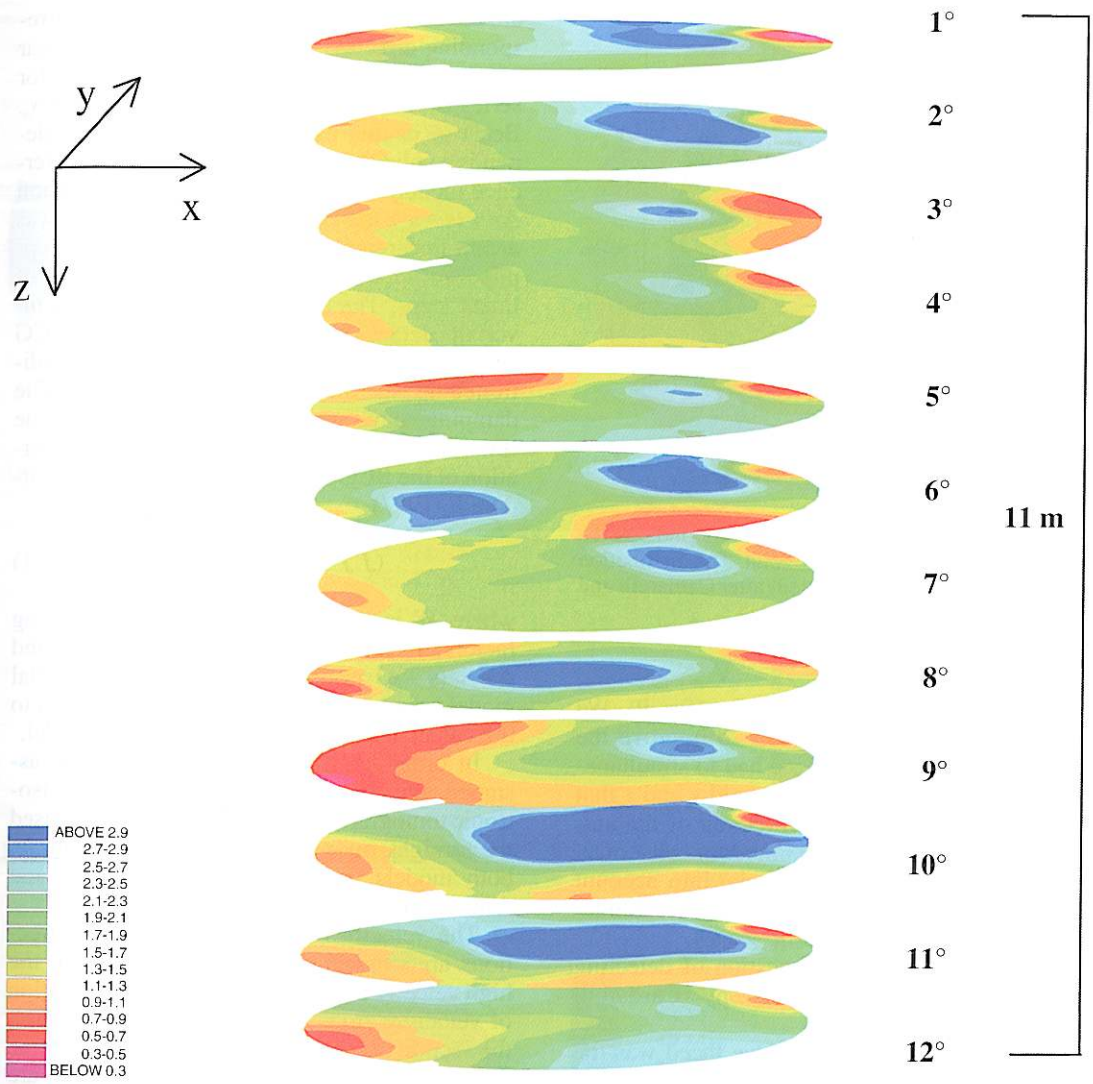

Fig. 8. Seismic 2D tomography results of Column A (after Cardarelli and de Nardis, 2001).

seismic tomography, in 2D projection, the wave travels perpendicularly to the mica and calcite beds and because the mica is weathered the wave is slower with respect to the head wave of seismic refraction that travels parallel to the calcite beds and gives back the velocity of calcite.

For this reason and because the investigated columns were restored, the survey was repeated on a third column performing a seismic anisotropic tomography.

The survey was carried out locating 13 sensors and 13 shot-points around a section of the column at a distance of 30 cm one from each

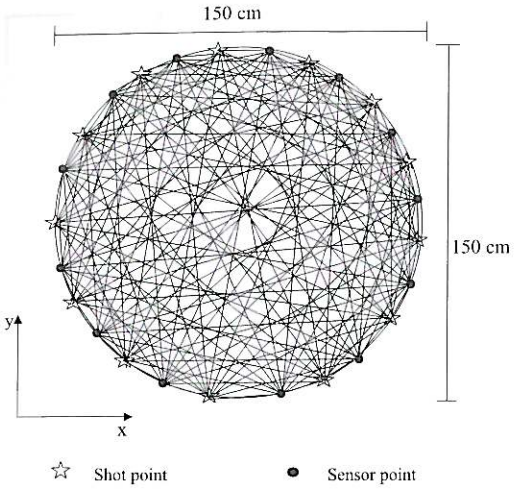

Fig. 9. Seismic tomography array. Points indicate the sensors the stars indicate shot point. The distribution of straight ray-paths is indicated (after Cardarelli and de Nardis, 2001).

other for a total of 169 ray-paths (fig. 9). We increased the number of paths to improve the angular coverage because we had to simultaneously invert the two slowness field s_x and s_y that corresponded to the main direction of the anisotropy. We increased the number of cells to 25, with variable dimensions to take into account the ray Fresnel theory considering the fundamental frequency of acoustic waves.

At first we faced the question of detecting the main directions of anisotropy (Cardarelli and de Nardis, 1998).

The second question that we faced was the choice of the algorithm to invert the data. We chose the algorithm proposed by Michelena *et al.* (1993). Michelena writes the travel-time equation as

$$t_i(s) = \sum_{j=1}^{N} \sqrt{\Delta x_{ij}^2 S_j^2 + \Delta y_{ij}^2 S_{j+N}^2}$$

where S_j are the slownesses in the main direction of the anisotropy, S_{j+N} are the slownesses in the perpendicular direction and Δx and Δy are the components of the ray-path in the corresponding directions. This equation is not linear and can be linearised by a first order Taylor series expansion centred in an initial model s_0. Because in this case the Jacobian matrix depends explicitly on the slowness of the reference model, and we computed the perturbation $\Delta \boldsymbol{s} = (\boldsymbol{s} - s_0)$, the estimation of the slowness was a non-linear problem. For this reason we applied an iterative method using a sequence of linear steps. The algorithm that we used to invert the data was the Biconjugate Gradient BCG (Press *et al.*, 1992). The system was preconditioned using variable damping factors. The damping values were defined by identifying the low velocity zones detected during the first iteration of the BCG algorithm (Bernabini and Cardarelli, 1997)

$$(\boldsymbol{J}^T\boldsymbol{J} + \boldsymbol{W})\Delta \boldsymbol{s} = \boldsymbol{J}^T\Delta \boldsymbol{t} \qquad (5.1)$$

where $\boldsymbol{W}$ is the diagonal matrix of damping factors; $\boldsymbol{J}$ is the Jacobian solution matrix; and $\Delta \boldsymbol{s} = (\boldsymbol{s} - s_0)$ is the perturbation to the initial model s_0 and $\Delta \boldsymbol{t} = \boldsymbol{t}(\boldsymbol{s}) - \boldsymbol{t}(s_0)$ is the correction to the calculated travel time of the initial model.

In order to compare the results of the assumed anisotropic model, we performed isotropic tomography using the same data. We used the straight ray-path approximation again. In both models we used the same number and dimensions of cells.

The velocity fields of the two main directions are shown in fig. 10a,b. In fig. 10a, the high velocity field (v_x) shows a marked variation of velocities from 0.8 to 4.8 km/s. In this case, the section of the column was divided into three zones. In the first zone where the velocities are lower (0.8 km/s), it is possible to locate these values in front of and behind the column where aligned cracks are present perpendicular to the schistosity. In the second zone, the velocity is between 1.2 and 2.4 km/s and in the third zone, the velocity reaches 4.8 km/s. The trend of velocity field is parallel to the schistosity of the material. In this case, the highest velocity value that we obtained is the same as that obtained using the seismic refraction method. It confirms the hypothesis on the anisotropic behaviour of the marble.

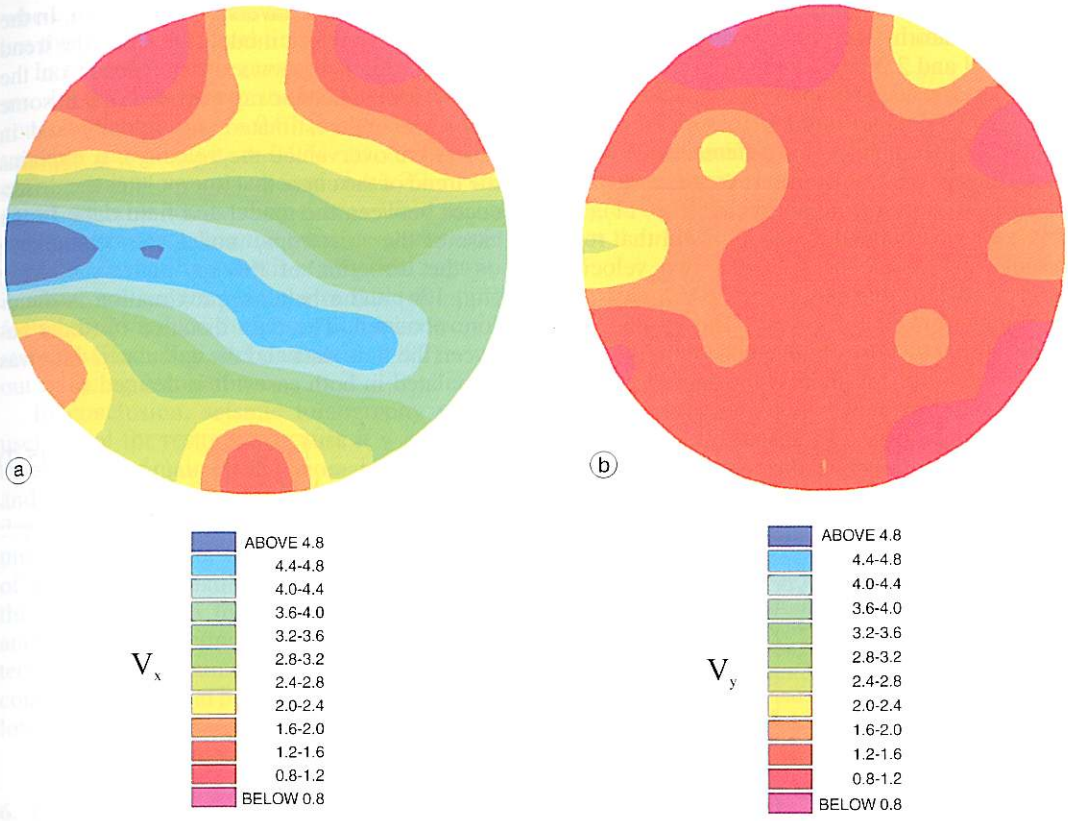

Fig. 10a,b. Column C. Seismic anisotropic results: a) V_x field; b) V_y field (after Cardarelli and De Nardis, 2001).

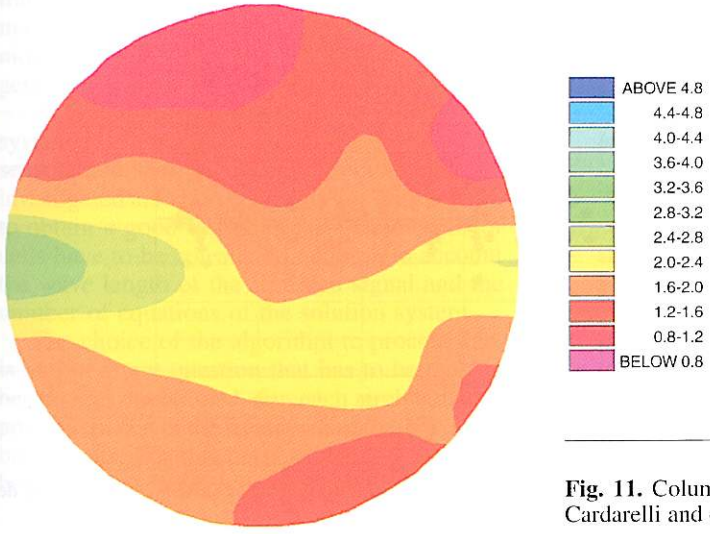

Fig. 11. Column C. Seismic isotropic results (after Cardarelli and de Nardis, 2001).

Figure 10b shows the low velocity field (v_y) as fairly uniform, the velocity values range between 0.8 and 2.0 km/s, with an average of 1.5 km/s. The low value of the velocity is due mainly to cracks parallel to the planes of the schistosity. In order to detect the differences between the isotropic and anisotropic results, we also performed isotropic tomography (fig. 11). In this case we obtained a velocity field that represents an average between the two velocity fields of the anisotropic case. The velocity values range from 0.6 to 2.8 km/s. These values are quite similar to those obtained in columns A and B. The trend of the field is the same as the v_x field because it shows the highest variation.

To compare the two results we considered the difference between the field data and the calculated data for both the isotropic and anisotropic tomographic inversion (fig. 12a,b). In the case of the isotropic model (fig. 12a), the trend of the difference shows a dependence on the direction in which the ray travelled (*i.e.* in some cases we underestimated the velocity and in others we overvalued the velocity). It explains the trend of the curve that interpolates the differences between the model and field data. In the case of the anisotropic model, the dependence on the direction of the ray-path is missing (fig. 12b) and a better approximation is therefore obtained. The data distance σ_t (d.d.) between the field data and the calculated data was calculated in both cases. It is defined as

$$\sigma_t = \sqrt{\frac{1}{M}\sum_{j=1}^{M}(t_f^j - t_c^j)^2} \qquad (5.2)$$

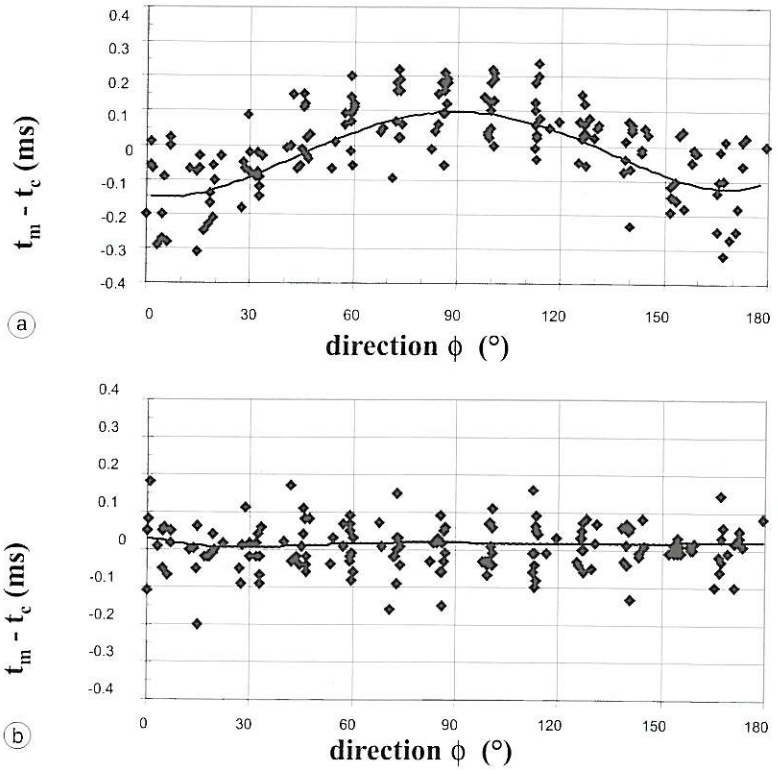

Fig. 12a,b. Data distance analysis: a) isotropic tomography; b) anisotropic tomography (after Cardarelli and de Nardis, 2001).

where the t_f are the measured travel times and t_c are the calculated travel times.

In the case of an isotropic model, $\sigma_t = 0.17$ ms. In the anisotropic model, in the case of constant damping, $\sigma_t = 0.07$ ms; in the case of variable damping, $\sigma_t = 0.054$ ms (this value corresponds to a mean error of about 7% of the mean value of the reading times). This was a new confirmation that the transversal isotropic model under the hypothesis of elliptical approximation, was accurate and the variable damping factor could reduce the errors and increase the stability (Bernabini and Cardarelli, 1997) without reducing resolution.

In conclusion, seismic tomography was a useful tool for restorers because it was able to determine the main elastic anomaly as location and dimensions of the weathered zones and the degree of degradation of the investigated columns. Furthermore, the anisotropic behaviour of the cipollino marble was detected. In the third column such hypothesis was confirmed and the main directions of anisotropy were detected with two main fields of velocities. Some considerations could be made about zones where low values of the velocities were singled out.

6. General conclusions

This short review on seismic high resolution transmission tomography aimed to highlight the main parameters and characteristics of the technique and describe some particular uses of this geophysics method.

At first, in order to obtain a well conditioned system it is necessary to plan the distribution of sensors and shot points and the division of the investigated area into cells. For this purpose and to obtain a good resolution, the dimensions of cells have to be considered taking into account the wave length of the recorded signal and the number of equations of the solution system.

The choice of the algorithm to process data is an important question that has to be tackled because as mentioned, for each problem it is possible to detect the fit algorithm that gives the best results. For this purpose the choice of the best damping factor is a question that has to be faced during processing to reach a good compromise between resolution and stability of the system.

As shown in the two case histories, seismic transmission tomography can be a valid tool to detect mechanical discontinuities in building structures (fractures, little cracks) and the decay degree of important monuments in order to redirect the restorer during restoration.

REFERENCES

BERNABINI, M. (1965): Alcune considerazioni sui rilievi sismici a piccole profondità, *Boll. Geofis. Teor. Appl.*, **7** (26), 106-119.

BERNABINI, M. and E. CARDARELLI (1987): Tomografia sismica con misure dirette di velocità, in *Atti del 6° Convegno Annuale GNGTS*, 595-607.

BERNABINI, M. and E. CARDARELLI (1997): Variable damping factors in travel time tomography, *J. Appl. Geophys.*, **38**, 131-141.

BERNABINI, M., M. CANCANICCIA and E. CARDARELLI (1990): Seismic survey of some pillars of Coliseum, in *Proceeding of 27th International Symposium on Archaeometry*, 677-686.

CARDARELLI, E. and R. DE NARDIS (1998): An application of travel time anisotropic seismic tomography for archaeological purpose, *EAGE-Extended Abstract of 60th Conference*, vol. 1.

CARDARELLI, E. and R. DE NARDIS (1999): The use of 3D and 2D seismic tomography for assessing the physical integrity of building panels, *Eur. J. Environ. Eng. Geophys.*, **3**, 131-142.

CARDARELLI, E. and R. DE NARDIS (2001): Seismic refraction, and isotropic and anisotropic seismic tomography on an ancient monument (Antonino and Faustina Temple A.D. 141), *Geophys. Prospect.*, **49**, 1-14.

CERVENY, V. and J.E.P. SOARES (1992): Fresnel volume ray tracing, *Geophysics*, **57** (7), 902-915.

GARDNER, L.W. (1939): An areal plan of mapping subsurface structure by refraction shooting, *Geophysics*, **4** (4).

MENKE, W. (1989): *Geophysical Data Analysis: Discrete Inverse Theory*, vol. 45.

MICHELENA, R.J., F. MUIR and J.M. HARRIS (1993): Anisotropic travel time tomography, *Geophys. Prospect.*, **41**, 381-412.

PAIGE, C.C. and M.A. SAUNDERS (1982): LSQR an algorithm for sparse linear equations and sparse least squares, in *ACM Trans. Math. Softw.*, edited by J.R. RICE, New York (U.S.A.), 43-71.

PRESS, H.W., S.A. TEUKOLSKY, W.T. VETTERLING and B.P. FLANNERY (1992): *Numerical Recipes in Fortran* (Cambridge University Press), 2nd edition, 71-82.

VAN DER SLUIS, A. and H.A. VAN DER VORST (1987): Numerical solutions of large sparse algebraic systems arising from tomographic problems, in *Seismic Tomography*, edited by G. NOLET (D. Reidel Publishing Company), 49-83.